Available online at www.sciencedirect.com
ScienceDirect
Polymer 49 (2008) 1693–1700
polymer
www.elsevier.com/locate/polymer

Polymorphism and β-form structure of poly(octamethylene 2,6-naphthalate)

Young Gyu Jeong [a], Kyu Jae Lee [a], Won Ho Jo [b], Sang Cheol Lee [a,*]

[a] School of Advanced Materials and Systems Engineering, Kumoh National Institute of Technology, 1 Yangho-Dong, Gumi 730-701, Republic of Korea
[b] Hyperstructured Organic Materials Research Center and School of Materials Science and Engineering, Seoul National University, Seoul 151-742, Republic of Korea

Received 4 September 2007; received in revised form 5 January 2008; accepted 14 January 2008
Available online 26 January 2008

Abstract

It was revealed that poly(octamethylene 2,6-naphthalate) (PON) existed in two different crystal structures, α- and β-form, depending on crystallization process: The α-form crystal was dominantly developed from the cold-crystallization, whereas the β-form was from the melt-crystallization. The apparent melting temperatures of α- and β-form crystals were characterized to be 175 and 183 °C, respectively. On the basis of X-ray diffraction and molecular modeling studies, the crystal structure of β-form, developed dominantly from the melt-crystallization, was identified to be triclinic with dimensions of $a = 0.601$ nm, $b = 1.069$ nm, $c = 2.068$ nm, $\alpha = 155.68°$, $\beta = 123.25°$, $\gamma = 52.85°$, and with the space group of $P\bar{1}$. The calculated crystal density was 1.243 g/cm^3, supporting that one repeating unit of PON exists in a unit cell. The octamethylene units in the PON backbone take largely *all-trans* conformation in the β-form unit cell.

Keywords: Crystal structure; Polymorphism; Thermal property

1. Introduction

There has been growing industrial and academic interest on poly(*m*-methylene 2,6-naphthalte)s (P*m*N, *m* indicates the number of methylene group), whose chemical structure is shown in Fig. 1, owing to their versatile applications as fibers, films, and engineered thermoplastic materials [1]. As expected, the naphthalene ring in P*m*N imparts greater rigidity to the polymer backbone compared to the benzene ring of polyesters, eventually attributing to their unique combination of excellent properties of thermal stability, chemical resistance, flame resistance, gas barrier property, mechanical strength, etc. Therefore, many studies on crystalline structures, crystallization, melting, and mechanical properties of P*m*Ns such as poly(ethylene 2,6-naphthalate) (PEN, $m = 2$) [2–7], poly(trimethylene 2,6-naphthalate) (PTN, $m = 3$) [8–10], poly(butylene 2,6-naphthalate) (PBN, $m = 4$) [11–15], poly(pentamethylene 2,6-naphthalate) (PPN, $m = 5$) [16], and poly(hexamethylene 2,6-naphthalate) (PHN, $m = 6$) [17] have been undertaken. With a continuing effort to investigate structures and properties of P*m*Ns, in an earlier work, we synthesized a series of P*m*Ns with various alkyl chain length of $m = 2$–6 and investigated their thermal and mechanical properties [18]. As a result, it was revealed that the thermal and mechanical properties of P*m*Ns are strongly influenced by the alkylene chain length of their backbones, exhibiting odd–even fluctuation of melting temperature and elastic modulus with increasing the number of methylene groups. On the other hand, although poly(octamethylene 2,6-naphthalate) (PON, $m = 8$), as a member of P*m*Ns, is also expected to be one of the promising crystalline polymeric materials for various applications, its fundamental characteristics such as crystalline structures, thermal and mechanical properties have not

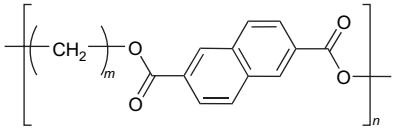

Fig. 1. Chemical structure of poly(*m*-methylene 2,6-naphthalate) (P*m*N).

* Corresponding author. Tel.: +82 54 478 7685; fax: +82 54 478 7710.
E-mail address: leesc@kumoh.ac.kr (S.C. Lee).

0032-3861/$ - see front matter © 2008 Elsevier Ltd. All rights reserved.
doi:10.1016/j.polymer.2008.01.044

been understood well until now. To discuss the structure–property relationship within a crystalline polymeric material based on the molecular structure, one must first determine the structure within the crystalline regions. Structural data stemming from crystalline regions of a polymer could provide detailed molecular organizations relevant to the overall microscopic and macroscopic physical properties of the material.

As the first step to understand the fundamental correlation between structure and property of PON, in this study, we synthesize a PON sample via melt-polycondensation and investigate its crystal structure and thermal properties by using X-ray diffraction, molecular modeling, and differential scanning calorimetry.

2. Experimental section

2.1. Synthesis and characterization of PON

PON was synthesized from 1,8-octanediol and 2,6-dimethyl naphthalate by two-step melt-condensation reactions using a catalyst of titanium isopropoxide. The first-step reaction was transesterification of 2,6-dimethyl naphthalate with 1,8-octanediol at 170 °C under nitrogen atmosphere and the second-step was a polycondensation reaction at 270 °C under high vacuum condition. At the end of reaction, the product in melt state was quenched into cold water and then dried in a vacuum oven for 24 h. PON synthesized in this study was used without further purification.

The intrinsic viscosity of PON was measured in a mixed solvent of phenol/1,1,2,2-tetrachloroethane (6/4, v/v) with an Ubbelohde viscometer at 35 °C. The intrinsic viscosity was found to be 0.62 dL/g, indicating that the sample has relatively high molecular weight enough to be processed in film or monofilament. Density measurement of crystalline or amorphous PON samples was carried out by using a density-gradient column with a series of mixed solutions of *n*-heptane (0.68 g/cm^3) and carbon tetrachloride (1.59 g/cm^3) at 25 °C. Thermal properties of a melt-quenched PON film were characterized with a Dupont 910 DSC at heating and cooling rates of 10 °C/min. The endothermic and exothermic peak temperatures were considered as the apparent melting and crystallization temperatures of PON, respectively.

2.2. X-ray measurements

One-dimensional (1D) X-ray diffraction patterns of PON films were obtained by using a Rigaku X-ray diffractometer with Cu-Kα radiation (40 kV and 200 mA) at a scanning rate of 2°/min. To confirm the existence of polymorphic structures of PON, two different sets of films were prepared by varying crystallization process (melt- and cold-crystallization) and temperature. For melt-crystallized samples, the films with 0.4 mm thickness were heated to the temperature of 30 °C higher than the melting temperature, held for 3 min in order to completely melt crystals, and then crystallized isothermally at various temperatures in the range of 90–170 °C from a few hours to several days. For cold-crystallized films, samples were heated to the temperatures at 200 °C for 3 min, quenched into cooled water of 0 °C, dried at 20 °C for one day, and finally annealed at an isothermal temperature in the range of 120–170 °C.

Two-dimensional (2D) X-ray fiber diagrams of PON monofilaments were recorded on a DIP2030 X-ray system (MAC Science Co.) with the flat imaging plate (3000 × 3000 pixels, 100 μm a pixel) as a detector and Cu-Kα radiation as an X-ray source (40 kV and 80 mA). For 2D X-ray fiber diagrams, PON monofilaments with 1.0 mm diameter were prepared by melt-spinning using a capillary rheometer (D8052, Kayeness Inc.), drawing uniaxially up to ~650% at a cross-head speed of 10 cm/min in a temperature-controlled chamber at 100 °C using a universal testing machine (Instron 4467, Instron Co.), and then annealing isothermally at various temperatures in the range of 130–170 °C under constant strain. The monofilament was arranged in the draw direction perpendicular to the X-ray beam and the sample to detector distance was 80 mm. All 1D and 2D X-ray measurements were performed at room temperature and the *d*-spacing was calibrated using a standard material of Si powder ($2\theta = 28.44°$).

Intensity distribution of all the reflections in a 2D X-ray fiber diagram were read out from X-ray diffraction data on the image plate and then stored as pixel data (3000 × 3000 pixels, 100 μm a pixel size) of Cartesian coordinates. The intensity of a diffraction spot is expressed as:

$$I = ALp\left|F(hkl)_{\mathrm{obs}}\right|^2 \exp\left(-2B\sin^2\theta/\lambda^2\right) \quad (1)$$

where A, L, p, $|F(hkl)_{\mathrm{obs}}|$, B, and l are the X-ray absorption coefficient, the Lorentz factor, the polarization factor, the observed structure factor, the isotropic temperature factor, and the X-ray wavelength, respectively. The experimentally observed structure factors ($|F(hkl)_{\mathrm{obs}}|$) were calculated from the intensity measurements of a 2D X-ray fiber diagram after removing the background intensity and correcting the Lorentz and polarization factors [19]. The absorption effect was not taken into account in this study. Unit cell parameters of a crystal structure were determined by a least-squares method with the preliminary cell dimensions obtained by a trial-and-error method.

2.3. Molecular modeling

Molecular modeling and X-ray diffraction simulation of a PON crystal structure were carried out with the aid of commercially available software (Cerius^2 version 4.6 by Accelrys, Inc.) on a Silicone Graphics Fuel workstation. The COMPASS force field [20] was applied to calculate the potential energy of a simulated crystal structure. The total potential energy of a molecular chain consists of contributions from intramolecular and intermolecular interactions. The intramolecular interactions include the bond stretching, valence angle bending, torsional, and inversion terms, and the intermolecular interactions consist of van der Waals and Coulomb terms. Standard bond lengths and angles for polyester were adopted to build the repeating unit. In modeling of a crystal structure, the

length of repeating unit(s) was adjusted to match with the experimentally-determined *c*-axis. The chain was then translated and rotated within a unit cell by minimizing the packing energy. During the energy minimization, the unit cell parameters were kept constant. Structure factors ($|F(hkl)_{cal}|$) were calculated from the energy-minimized crystal structure model. The scale factor and overall isotropic temperature factor were refined to minimize the difference between the structure factors ($|F(hkl)_{cal}|$) of the modeled crystal structure and the ones ($|F(hkl)_{obs}|$) observed experimentally. The reasonability of a finally modeled crystal structure was evaluated by using the following discrepancy factor (R):

$$R = \frac{\sum \left| |F(hkl)_{obs}| - |F(hkl)_{cal}| \right|}{\sum |F(hkl)_{obs}|} \times 100(\%). \quad (2)$$

3. Results and discussion

3.1. Polymorphism and thermal properties of PON

To identify the possibility of PON polymorphism by crystallization process and temperature, 1D X-ray diffraction patterns of the film samples obtained by cold- and melt-crystallization at a variety of temperatures were collected. Fig. 2 shows X-ray diffraction patterns of the PON films melt-crystallized isothermally at various temperatures. All the samples melt-crystallized displayed consistent diffraction peaks at 10.30, 12.94, 18.36, 20.98, 23.40, and 26.24°, regardless of the crystallization temperature. On the other hand, 1D X-ray diffraction patterns of the cold-crystallized films are totally different from the patterns of the samples melt-crystallized, as shown in Fig. 3. For the samples cold-crystallized, diffraction peaks at 14.80, 16.20, 19.70, 20.68, and 24.26° are detected distinctively at various crystallization temperatures. Therefore, it is reasonable to contend that PON exists in two different crystal structures, depending on the crystallization process. In this study, the crystal structure developed from the cold-crystallization is designated as α-form, and the structure from the melt-crystallization is β-form. We expect that the existence of different crystal structures for PON stems from the different nucleation processes of α- and β-form according to the cold- and melt-crystallization methods. Unlike the diffraction patterns of the films melt-crystallized, the diffraction peaks of the films cold-crystallized were observed to be very board, indicating that the crystal sizes of samples from cold-crystallization are relatively small, compared to those of ones melt-crystallized. On the other hand, the diffraction peaks of the samples cold-crystallized become sharper with increasing the cold-crystallization temperature. In addition, the film cold-crystallized at 170 °C exhibits diffraction peaks corresponding to β-form, as can be seen in Fig. 3. It means that partial β-form crystals are also developed at higher crystallization temperatures, despite the cold-crystallization process. Also, it should be mentioned that, although the β-form is the dominant crystal structure for the melt-crystallized samples, as shown in Fig. 2, the samples melt-crystallized at 90 and 100 °C exhibit a tiny but discernable diffraction peak at 19.70°, which corresponds to the α-form.

Fig. 4 shows DSC heating and cooling thermograms of a sample melt-quenched to 0 °C. Closer examination of the first heating thermogram (Fig. 4a) revealed that a small

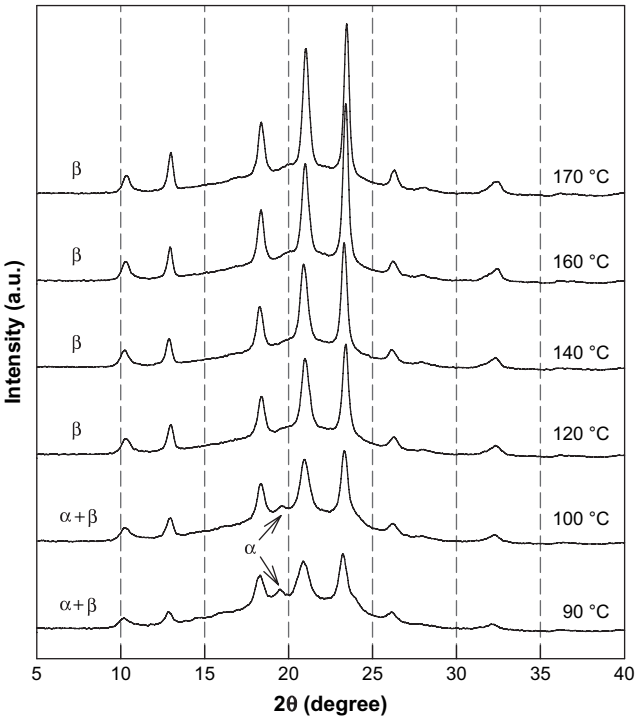

Fig. 2. 1D X-ray diffraction patterns of PON films melt-crystallized isothermally at various temperatures in the range of 90–170 °C.

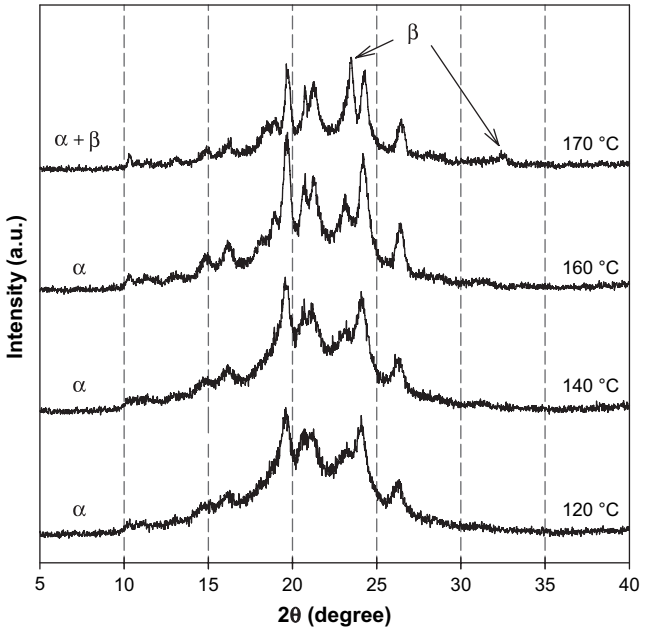

Fig. 3. 1D X-ray diffraction patterns of PON films cold-crystallized isothermally at various temperatures in the range of 120–170 °C.

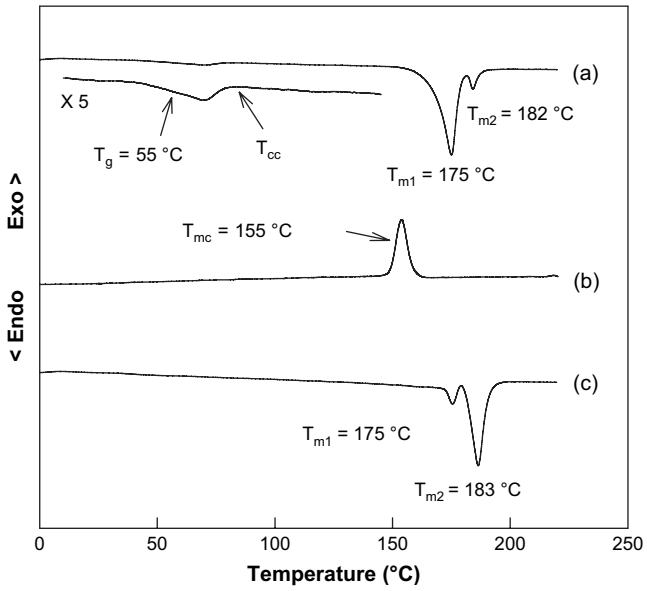

Fig. 4. DSC thermograms of the melt-quenched PON film at heating and cooling rates of 10 °C/min: (a) the first heating run; (b) the first cooling run; (3) the second heating run after cooling.

cold-crystallization exotherm appears at around 70 °C just above the glass transition temperature of 55 °C. It demonstrates that PON exhibits very rapid crystallization behavior. In addition, the heating thermogram shows two melting endotherms at 175 and 182 °C, as can be seen in Fig. 4a. It is speculated that the intense melting endotherm at 175 °C originates from the α-form crystals developed during the cold-crystallization of quenched sample and the weak melting endotherm at 182 °C originates from the β-form crystals formed during melt-quenching. In the cooling thermogram of Fig. 4b, there is only one crystallization exotherm at 155 °C. After cooling at a rate of 10 °C/min, the sample was subsequently heated, as represented in Fig. 4c. It is considered that the intense melting endotherm at 183 °C is due to the melting of β-form crystals developed dominantly from the melt during the slow cooling and the weak melting endotherm at 175 °C is due to the melting of α-form crystals developed during the cooling and/or heating process.

3.2. Crystal structure determination of PON β-form

In order to determine the crystal structures of α- and β-form, we obtained 2D X-ray fiber diagrams of monofilaments which were oriented uniaxially and annealed isothermally at various temperatures, as can be seen in Fig. 5. Except for the sample annealed at 170 °C, reflections in X-ray fiber diagrams of the samples annealed at 130 and 150 °C were quite unclear, which is believed to originate from the small crystal

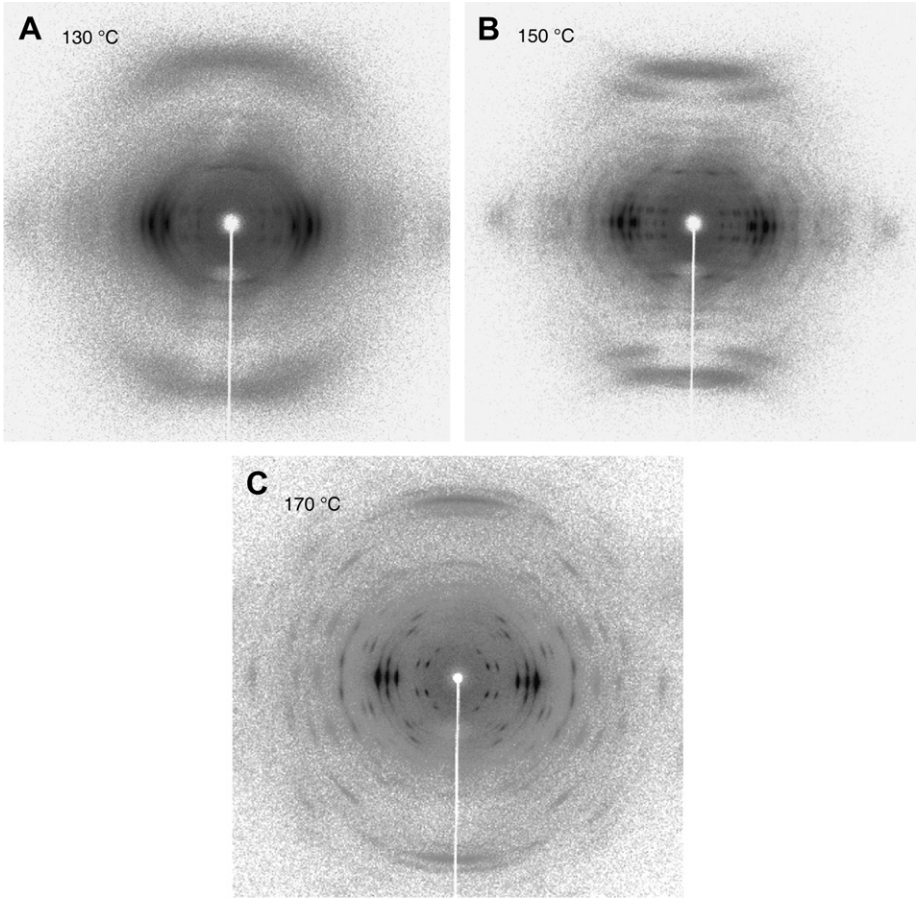

Fig. 5. 2D X-ray fiber diagrams of PON monofilaments drawn uniaxially to the strain of 650% and annealed isothermally at various temperatures under constant strain.

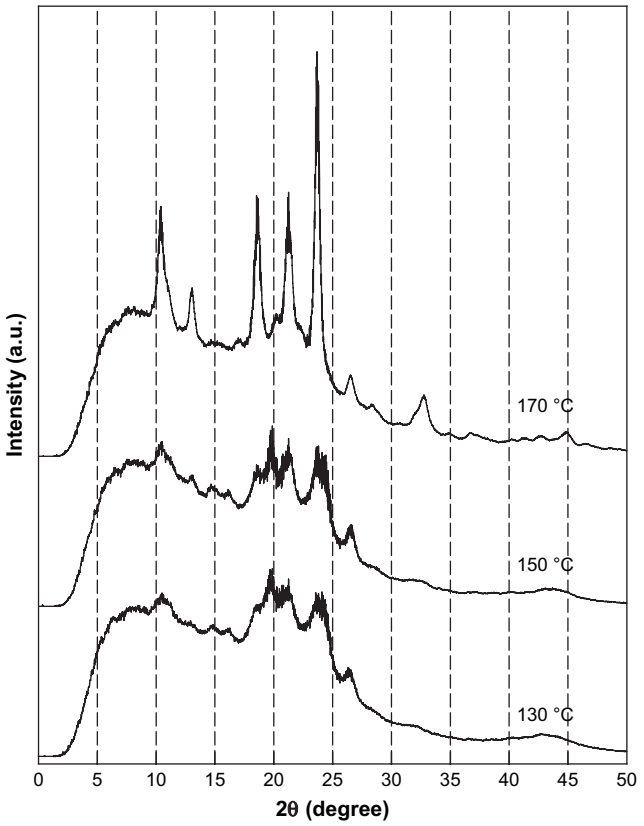

Fig. 6. X-ray fiber diffractograms of PON monofilaments drawn uniaxially and annealed isothermally at various temperatures under constant strain, which were obtained by integrating circularly the 2D X-ray fiber diagrams shown in Fig. 5.

sizes and low sample crystallinity. When 1D X-ray diffractograms were obtained by integrating circularly the 2D fiber diagrams, as can be seen in Fig. 6, it was found that the monofilament annealed at 170 °C is only composed of the β-form crystals, while the samples at 130 and 150 °C are dominantly composed of α-form crystals. On the other hand, it was unfortunate that, for monofilament annealed at 130 and 150 °C, we could not get clear 2D X-ray fiber diagrams (Fig. 5A and B) enough to determine the crystal structure of α-form. Therefore, in this study, the β-form crystal structure was just analyzed using the X-ray fiber diagram (Fig. 5C) which showed clearly identified reflections. Since the 2D X-ray fiber diagram of the β-form in Fig. 5C shows the well-layered diffraction patterns, we could calculate the distance between the first layer and the equatorial line, which is suggestive of a crystallographic *c*-axis length. The resulting *c*-axis length of the β-form crystal structure was determined to be 2.068 nm. This value was found to be comparable to the repeat distance of a fully extended conformation of PON backbone. Therefore, it is valid to assume that the octamethylene sequences in β-form crystal lattices take *all-trans* conformation.

Indexing of diffraction spots in the X-ray fiber diagram in Fig. 5C yields a triclinic unit cell for β-form with dimensions of $a = 0.601$ nm, $b = 1.069$ nm, $c = 2.068$ nm, $\alpha = 155.68°$, $\beta = 123.25°$, and $\gamma = 52.85°$. The crystal density of β-form

Table 1
Comparison of the calculated *d*-spacings and structure factors of the PON β-form with the experimentally observed values

hkl	d_{cal} (nm)	d_{obs} (nm)	$\lvert F(hkl)_{cal}\rvert$		$\lvert F(hkl)_{obs}\rvert$
100	0.479	0.478	54.8		50.8
010	0.420	0.420	73.6		77.9
110	0.377	0.376	101.7		106.1
$1\bar{1}0$	0.277	0.275	9.3		17.5
210	0.242	0.239	12.4	19.4	20.4
200	0.240		14.9		
120	0.218		38.2		
220	0.189	0.187	37.7	38.9	46.4
$2\bar{1}0$	0.185		9.6		
001	0.852	0.854	24.2		
$01\bar{1}$	0.676	0.678	18.2		
$11\bar{1}$	0.530		6.6		
101	0.419	0.416	36.8	55.1	58.3
$10\bar{1}$	0.416		41.0		
011	0.290		16.3		
111	0.275	0.273	57.2	59.4	63.5
$21\bar{1}$	0.271		16.0		
$02\bar{1}$	0.264		6.4		
201	0.231		13.8		
$20\bar{1}$	0.230		9.6		
$1\bar{1}\bar{1}$	0.227		23.7		
211	0.207		22.7		
$01\bar{2}$	0.830	0.821	5.6		3.7
$11\bar{2}$	0.591		4.9		5.4
$12\bar{2}$	0.374	0.375	4.9		
$02\bar{2}$	0.338	0.337	21.2	24.2	21.4
$1\bar{1}2$	0.338		11.6		
102	0.319	0.317	11.4	27.2	29.5
$10\bar{2}$	0.317		24.7		
$21\bar{2}$	0.278	0.274	30.6	31.3	27.7
$22\bar{2}$	0.265		6.7		
112	0.212	0.209	7.5	39.1	31.1
$13\bar{2}$	0.209		12.9		
$20\bar{2}$	0.208		36.1		
$03\bar{2}$	0.191		8.2		
$1\bar{1}2$	0.188		30.2		
$01\bar{3}$	0.536	0.529	7.1		4.2
$12\bar{3}$	0.481	0.478	6.2		7.9
$11\bar{3}$	0.451	0.449	17.5		23.2
$1\bar{1}3$	0.305		10.6		
$22\bar{3}$	0.295		18.5		
003	0.284	0.281	20.5		25.9
$21\bar{3}$	0.258		8.4		
$13\bar{3}$	0.257		7.3		
$1\bar{2}3$	0.249	0.246	15.1	21.1	15.9
103	0.245		14.8		
$03\bar{3}$	0.225	0.224	16.8		15.4
$32\bar{3}$	0.191		11.7		
$12\bar{4}$	0.484	0.479	4.8		2.7
$02\bar{4}$	0.415	0.409	18.0		23.4
$01\bar{4}$	0.348	0.337	6.0	12.7	10.7
$11\bar{4}$	0.321		11.2		
$13\bar{4}$	0.314	0.312	18.7		15.8
$22\bar{4}$	0.296	0.293	11.2		8.0
$23\bar{4}$	0.264		6.6		
$03\bar{4}$	0.261		11.3		
$1\bar{2}4$	0.249		20.1		
$21\bar{4}$	0.224	0.224	6.6		3.1
004	0.213		6.5		
$1\bar{3}4$	0.189		26.4		
$24\bar{4}$	0.187		13.4		
$12\bar{5}$	0.379	0.377	6.1		4.2

(*continued*)

Table 1 (*continued*)

hkl	d_{cal} (nm)	d_{obs} (nm)	$\lvert F(hkl)_{cal}\rvert$		$\lvert F(hkl)_{obs}\rvert$
$13\bar{5}$	0.354	0.361	3.5		1.7
$02\bar{5}$	0.343	0.336	18.5		
$23\bar{5}$	0.287	0.275	6.7	15.9	10.9
$22\bar{5}$	0.266		14.4		
$01\bar{5}$	0.252		16.4		
$12\bar{5}$	0.231		8.1		
$11\bar{5}$	0.208		19.1		
$33\bar{5}$	0.200		18.1		
$13\bar{5}$	0.197		20.4		
$04\bar{5}$	0.189		8.5		

crystal calculated from the unit cell parameter is 1.243 g/cm^3, which is close to the experimental value of 1.232 g/cm^3 determined using the following equation:

$$\frac{1}{\rho} = \frac{x_c}{\rho_{cr}} + \frac{1 - x_c}{\rho_{am}} \tag{3}$$

where, x_c, ρ, ρ_{cr}, and ρ_{am} are the degree of crystallinity determined by X-ray measurement, the density of sample, the density of crystalline phase, and the density of amorphous phase, respectively. For the PON film melt-crystallized isothermally at 170 °C for 1 h, the crystallinity and density was 32.4% and 1.173 g/cm^3, respectively. The density of a melt-quenched amorphous PON sample (ρ_{am}) was measured to be 1.146 g/cm^3. Therefore, it can be assumed that, from the density evaluated experimentally, one polymer chain passes through the a–b plane of the unit cell. When an initial structural model of the β-form was energy-minimized in a primarily determined unit cell without any symmetry constraint, it was found that the final energy-minimized β-form structure satisfies the symmetry condition of $P\bar{1}$. As the result, the midpoint of naphthalene ring and the central CH_2–CH_2 bond of octamethylene unit are correspondents to centers of symmetry along c-axis. Furthermore, all bond lengths, bond angles and torsion angles in the polymer backbone should be symmetric based on these centers of symmetry. The structure factors and d-spacings calculated from the energetically-minimized β-form model and the experimental 2D X-ray fiber diagram are summarized in Table 1. When the experimentally observed structure factors ($\lvert F(hkl)_{obs}\rvert$) were compared with the structure factors ($\lvert F(hkl)_{cal}\rvert$) calculated from the energy-minimized model, the discrepancy factor of R was 15.6%. In the refinement, the overall isotropic temperature factor of 5.1 Å^2 was used. On the basis of a chemical repeat unit of PON with the numbering of atoms (Fig. 7), fractional coordinates of atoms in the β-form unit cell are assigned and summarized in Table 2. It is revealed that the torsion angles of the chain backbone in the β-form unit cell are to be C_4–C_3–C_6–

Table 2
Fractional coordinates of atoms in the β-form unit cell

Atom	*x*/*a*	*y*/*b*	*z*/*c*
C1	−0.0990	0.0293	−0.0126
C2	0.1220	−0.0424	0.0801
C3	−0.0408	−0.0153	0.1225
C4	−0.2325	0.0570	0.0975
C5	−0.2622	0.0719	0.0319
C6	−0.0113	−0.0201	0.1931
C7	−0.2107	−0.0206	0.2940
C8	−0.0744	0.0477	0.3459
C9	−0.1085	−0.0179	0.4112
C10	0.0151	0.0387	0.4690
O1	0.1464	−0.0683	0.2202
O2	0.1894	0.0216	0.2282
H2	0.2735	−0.0883	0.0981
H4	−0.3657	0.0907	0.1297
H5	−0.4143	0.1171	0.0136
H7[a]	−0.3887	−0.0107	0.3058
H7′[a]	−0.1729	−0.1212	0.2967
H8	0.1037	0.0467	0.3329
H8′	−0.1251	0.1466	0.3485
H9	−0.2884	−0.0202	0.4223
H9′	−0.0554	−0.1162	0.4059
H10	0.1943	0.0459	0.4577
H10′	−0.0451	0.1349	0.4774

[a] H7 and H7′ indicate hydrogen atoms which are covalent-bonded to C7.

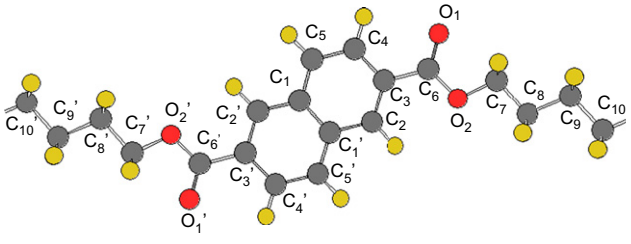

Fig. 7. Schematic representation of a repeat unit of PON and numbering of atoms.

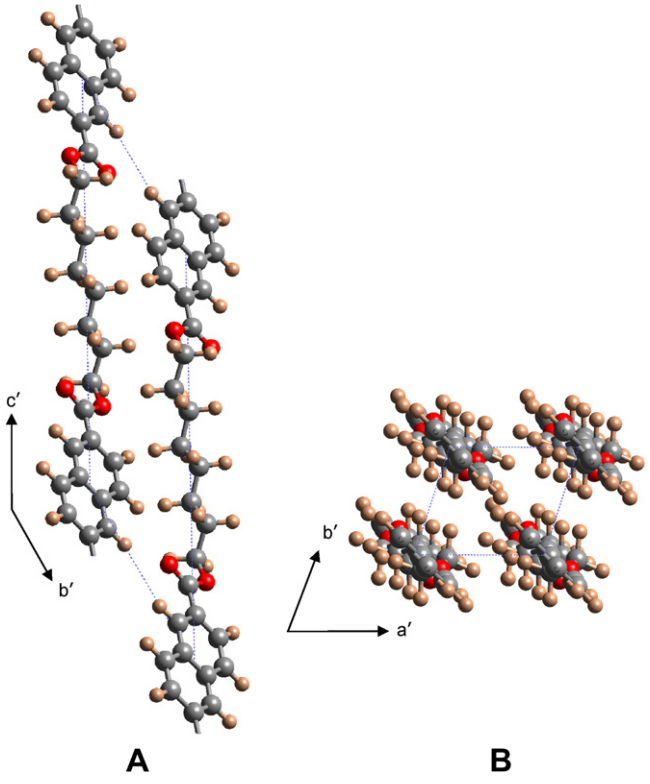

Fig. 8. Molecular packing in the β-form unit cell: (A) projection along a-axis; (B) projection along c-axis.

$O_2 = -[C_4'-C_3'-C_6'-O_2'] = -177.5°$, $C_3-C_6-O_2-C_7 = -[C_3'-C_6'-O_2'-C_7'] = 163.8°$, $C_6-O_2-C_7-C_8 = -[C_6'-O_2'-C_7'-C_8'] = 81.9°$, $O_2-C_7-C_8-C_9 = -[O_2'-C_7'-C_8'-C_9'] = -175.9°$, $C_7-C_8-C_9-C_{10} = -[C_7'-O_8'-C_9'-C_{10}'] = -179.7°$, $C_8-C_9-C_{10}-C_{10}' = -[C_8'-O_9'-C_{10}'-C_{10}] = -175.7°$, and $C_9-C_{10}-C_{10}'-C_9' = 180.0°$. It is of suggestive that carboxylic groups are nearly coplanar to the naphthalene ring plane and also the aliphatic octamethylene unit takes nearly *all-trans* conformation. On the other hand, it should be noted that the naphthalate groups are slightly distorted to the octamethylene units because the torsion angle of $C_6-O_2-C_7-C_8$ is 81.9°. From the final model of the β-form crystal structure shown in Fig. 8, it can be recognized that the aromatic groups are in face-to-face arrangement and the chain packing is of the parallel type. When a 2D X-ray fiber diagram was simulated from the β-form crystal structure determined by molecular modeling and mechanics, as shown in Fig. 9A, it was revealed to be quite similar to the experimental X-ray fiber diagram of Fig. 9B.

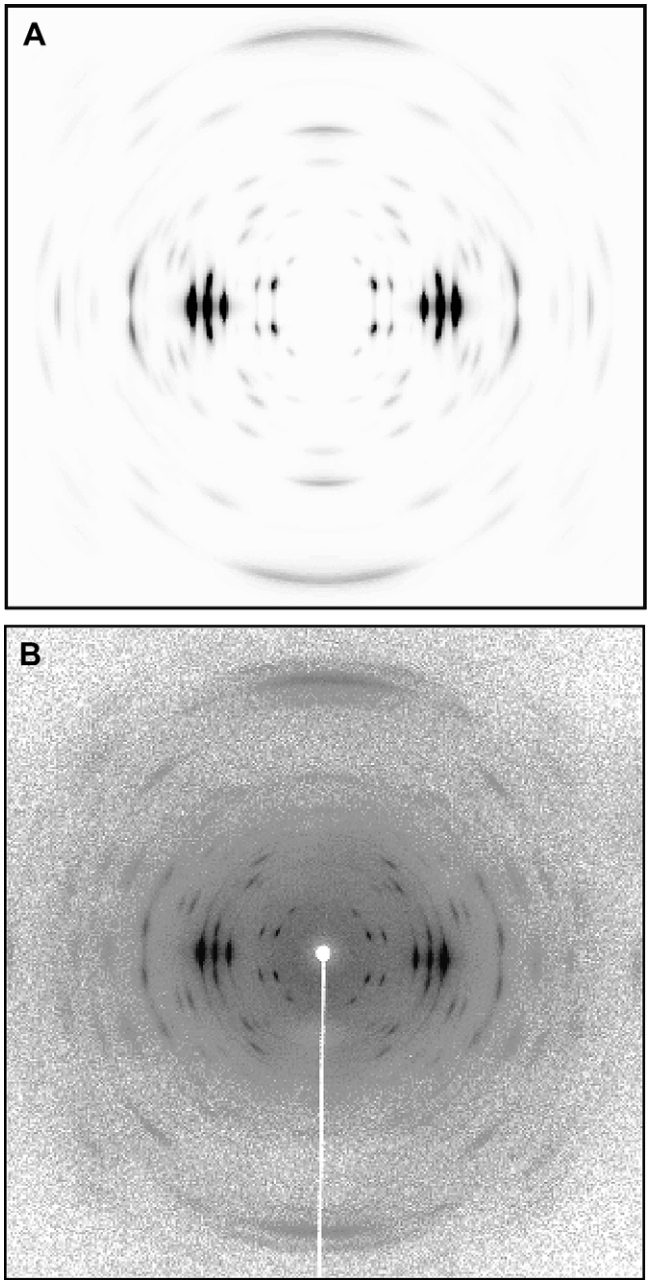

Fig. 9. Comparison of (A) a simulated 2D X-ray fiber diagram (an angular deviation of 5° from the perfect orientation) of the β-form crystal structure with (B) an experimental X-ray fiber diagram.

4. Conclusions

It was identified that PON has two different crystal structures of α- and β-form, depending on the crystallization process. The α-form was developed dominantly from the cold-crystallization, while the β-form was from the melt-crystallization. It was found from thermal analysis that the apparent melting temperatures of α- and β-form crystals were characterized to be 175 and 183 °C, respectively. It demonstrated that PON has relatively high melting temperature, in spite of the long alkyl chain in its backbone. On the basis of X-ray fiber diffraction and molecular modeling studies, the unit cell of the β-form crystal was determined to be a triclinic with unit cell dimensions of $a = 0.601$ nm, $b = 1.069$ nm, $c = 2.068$ nm, $\alpha = 155.68°$, $\beta = 123.25°$, and $\gamma = 52.85°$. The crystal density (1.243 g/cm^3) calculated from the simulated β-form crystal structure was found to be similar with the value (1.232 g/cm^3) evaluated experimentally, which indicates that the unit cell contains one repeating unit. The chain in the β-form unit cell possesses two crystallographic centers of symmetry, supporting that the space group is $P\bar{1}$. In the β-form crystals, the octamethylene unit takes nearly *all-trans* conformation and the packing mode between the naphthalene rings is of the face-to-face type. The detailed crystal structure of α-form and the transformation mechanism between α- and β-form are under investigation, which will be reported in near future.

Acknowledgements

This paper was supported by Research Fund, Kumoh National Institute of Technology.

References

[1] Duling IN. W.C. United States 3436376; 1969.
[2] Buchner S, Wiswe D, Zachmann HG. Polymer 1989;30(3):480–8.
[3] Cakmak M, Wang YD, Simhambhatla M. Polym Eng Sci 1990;30(12):721–33.
[4] Cakmak M, Lee SW. Polymer 1995;36(21):4039–54.
[5] Lee WD, Yoo ES, Im SS. Polymer 2003;44(21):6617–25.
[6] Martins CI, Cakmak M. Macromolecules 2005;38(10):4260–73.
[7] Nam JY, Fukuoka M, Saito H, Inoue T. Polymer 2007;48(8):2395–403.
[8] Jeong YG, Jo WH, Lee SC. Polymer 2003;44(11):3259–67.
[9] Jeong YG, Jo WH, Lee SC. Polymer 2004;45(2):379–84.
[10] Liang Y, Lee HS. Macromolecules 2005;38(23):9885–8.
[11] Lee SC, Yoon KH, Kim JH. Polym J 1997;29(1):1–6.
[12] Koyano H, Yamamoto Y, Saito Y, Yamanobe T, Komoto T. Polymer 1998;39(18):4385–91.
[13] Papageorgiou GZ, Karayannidis GP. Polymer 2001;42(6):2637–45.
[14] Tashiro K, Cheng J, Ike M. Macromolecules 2003;36(2):359–67.

[15] Yasuniwa M, Tsubakihara S, Fujioka T. Thermochim Acta 2003;396(1–2):75–8.
[16] Jeong YG, Jo WH, Lee SC. Polymer 2002;43(26):7315–23.
[17] Jeong YG, Jo WH, Lee SC. Polym J 2001;33(12):913–9.
[18] Jeong YG, Jo WH, Lee SC. Polymer 2004;45(10):3321–8.
[19] Tashiro K, Asanaga H, Ishino K, Tazaki R, Kobayashi M. J Polym Sci Part B Polym Phys 1997;35(11):1677–700.
[20] Sun H. J Phys Chem B 1998;102(38):7338–64.